Modular Redox Switching of Dinuclear Organometallic Molecular Junctions

Yuya Tanaka,*[1,2]† Naoki Morozumi,[2]† Tatsuhiko Ohto,[3,4] Satoshi Kaneko,[5] Yasuhisa Naitoh,[6] Hirokazu Tada,[3] Shintaro Fujii,[5] Tomoaki Nishino,[5] Munetaka Akita*[1,2]

[1]Laboratory for Chemistry and Life Science, Institute of Innovative Research, Tokyo Institute of Technology, 4259 Nagatsuta, Midori-ku, 226-8503, Yokohama, Japan.

[2] Department of Chemical Science and Engineering, School of Materials and Chemical Technology, Tokyo Institute of Technology, 4259 Nagatsuta, Midori-ku, 226-8503, Yokohama, Japan.

[3] Graduate School of Engineering Science, Osaka University

1-3 Machikaneyama, Toyonaka, Osaka 560-8531, Japan

[4] Center for Quantum Information and Quantum Biology, Institute for Open and Transdisciplinary Research Initiatives, Osaka University, 1-3 Machikaneyama, Toyonaka, Osaka 560-8531, Japan

[5] Department of Chemistry, School of Science, Tokyo Institute of Technology, 2-12-1 Ookayama, Meguro-ku, 152-8551, Tokyo, Japan.

[6] National Institute of Advanced Industrial Science and Technology (AIST), Tsukuba, Ibaraki 305-8565, Japan

ABSTRACT: Molecular switch is one of the essential functional units of molecular electronics. Here, we report development of new molecular switches based on the electron-rich diruthenium complexes with the (2,5-di-R-substituted 1,4-diethynylbenzene)diyl linkers. The dinuclear molecular switches, {μ-p-C≡C-(2,5-R_2-C_6H_2)-C≡C}{Ru(dppe)$_2$(C≡C-C_6H_4-p-SMe)}$_2$ **1^R** (R= OMe, H, CF$_3$), with various substituents (R) on the bridging phenylene rings showed two successive reversible 1e-oxidation waves, indicating stability of 1e-oxidized mixed-valence species. The solid-state structure of [**1^H**]$^+$ showed the charge-localized Robin-Day class II nature, while that of [**1^{OMe}**]$^+$ revealed the fully charge-delocalized class III nature. These characters were also evident from the spectroscopic data in solutions. Single-molecule conductance measurements by the scanning tunneling microscope break junction method revealed a significant dependence of the conductance on R, i.e. **1^{OMe}** turned out to be >100-times more conductive than **1^H** and **1^{CF3}**, whereas the substituent effect of the monocationic complexes was within a fold-change of 2. As a result, the ON/OFF ratios (the ratios of the conductance of the cationic species [**1^R**]$^+$ to that of the neutral species **1^R**) were critically dependent on R (as large as 191 when R = CF$_3$) and even reversed (0.4 when R = OMe). Furthermore, the neutral and monocationic complexes **1^H** and [**1^H**]$^+$ fabricated into the nanogap devices showed *in situ* ON/OFF switching behavior. The present study demonstrates not only the rare examples of the mixed-valence complexes which were subjected to the break junction measurements but also the first examples of molecular switch, the ON/OFF ratio of which was controlled by tuning the organic linker parts.

INTRODUCTION

Molecular switch, which can control a specific function of itself by an external stimulus reversibly, is an essential part in molecule-based electronics. So far, there have been reports on various molecular switches incorporated into metal-molecule-metal junctions, which are responsive to mechanical,[1–3] acid-base,[4,5] photo-irradiation[6–8], and redox stimuli[9,10]. Redox stimulus is superior to other stimuli due to the easy fabrication of the trigger by installation of a third electrode into nano-devices, in addition to drain and source electrodes.[11] Some redox-triggered organic molecular switches have been known. Neaton, Venkataraman, and Campos reported an aromatic bifluorenylidene-based redox switch, which was converted to the anti-aromatic dicationic states upon 2e-oxidation (Figure 1a).[10] A large ON/OFF ratio (the ratio of the conductance of the ON and OFF states) with a factor of 70 was reported. Multiple switching behavior was reported for the naphthalenediimide derivative (Figure 1b).[9] Stepwise 1e-reduction led to the mono- and di-anionic states and the monoanionic state showed conductance 10 times higher than that of the neutral state. For the redox switch, however, there remain two key issues to be solved. One is the instability of the oxidized or reduced radical species formed upon application of redox stimuli. The other is lack of rational molecular design to modulate/control the ON/OFF ratio without interfering the original switching function.[12]
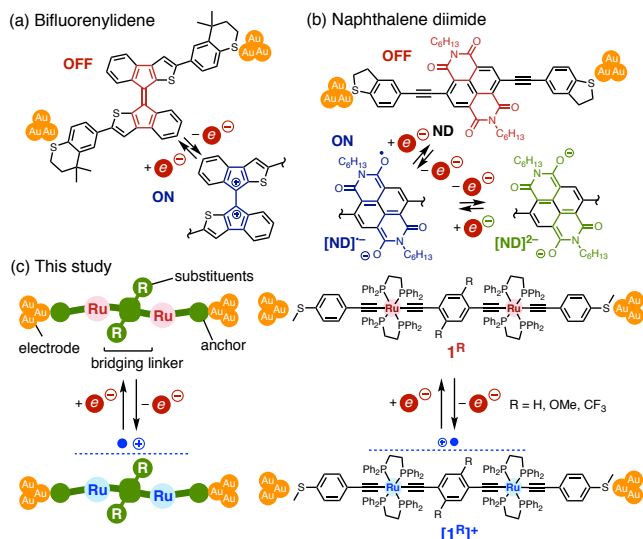
Figure 1. Organic Molecular switches based on (a) bifluorenylidene and (b) naphthalene diimide. (c) Concept of the present redox-responsive dinuclear molecular switches **1^R**-**[1^R]^+** (R = OMe, H, CF$_3$).

Of mixed-valence (MV) species, dinuclear systems are composed of two metal centers with different oxidation states (M/M$^{\bullet+}$), in many cases, bridged by an organic ligand (BL),[13] i.e. M-BL-M$^{\bullet+}$, and are considered to be excellent model systems to examine the Marcus-type charge transfer phenomena in solution. A charge carrier can be transferred from one metal center to the other metal center with a different oxidation state through the BL. 1e-Redox process of a closed-shell precursor (M-BL-M) leads to an open-shell MV complex, which may be stabilized by charge delocalization over the [M-BL-M]$^{\bullet+/-}$ backbone. This redox interconversion between the neutral and MV states could be used as a guiding principle for molecular switch not only because the two electronic states are drastically different but also because the charge transfer phenomena can be finely controlled by appropriate combination of the metal fragments and the bridging ligand, which should affect the conductance through the molecular junction based on the MV systems. Furthermore, the effect of charge-localization of MV complexes on the single-molecule conductance study remains elusive.

Transition-metal acetylides are a class of promising candidates for components of molecular electronics as they show highly conducting nature due to the high-lying HOMO energy levels caused by the electron-rich metal fragments with *nd* electrons.[14–17] In addition, many of them are redox-active and, therefore, can be the switching triggers. Thus far, the redox-switching behavior of organometallic mononuclear acetylide complexes in nanogaps has been investigated only for *in-situ* charging/discharging at low temperature.[18–20] However, no example operated at room temperature has been reported mainly because of the intrinsic instability of the oxidized/reduced open-shell radical species of *mononuclear* organometallic complexes.[21,22] Herein we report new redox-switchable *dinuclear* organometallic complexes based on the electron-rich *trans*-Ru(dppe)$_2$ fragments **1^R** (dppe: 1,2-bis(diphenylphosphino)ethane, Figure 1c). The following two advantages are noted for the (diethynylbenzene)diyl

diruthenium complexes with the Ru-C≡C-*p*-C$_6$H$_4$-C≡C-Ru core skeletons: (1) the 1e-oxidized monocationic species can be stabilized by the diruthenium structures due to the formation of stable MV states and (2) the electronic properties of the neutral and monocationic species can be finely modulated by substituents on the central phenylene moiety.[23]

RESULTS AND DISCUSSION

Synthesis and Characterization of Neutral Complexes 1^R. We have synthesized the diruthenium acetylide complexes **1^R** (R = OMe, H, CF$_3$) through coupling between the mononuclear chloro precursor with the SMe-terminated acetylide ligand and appropriate 2,5-disubstituted 1,4-diethynylbenzenes in 30-72 % yields in a manner similar to the method reported previously.[24–26] The obtained diruthenium complexes **1^R** were fully characterized through conventional spectroscopic methods including nuclear magnetic resonance (NMR), infrared and high-resolution mass spectroscopy, and elemental analyses. Single sets of ^{1}H (Figure 2b) and ^{31}P{^{1}H} NMR signals (δ_p ~54 ppm, See SI) indicate highly symmetric structures. ν(C≡C) vibration frequencies observed around 2060 cm^{-1} are comparable to those of the relevant ruthenium acetylides.[24,25] The X-ray structure of **1^H** shown in Figure 2c reveals a rigid rod-like structure, and the Ru-Ru and S-S distances were 12.190 and 30.819 Å, respectively. The Ru-C (2.040 Å) and C≡C (1.219 Å) bond lengths are within the ranges of those reported previously.[25]
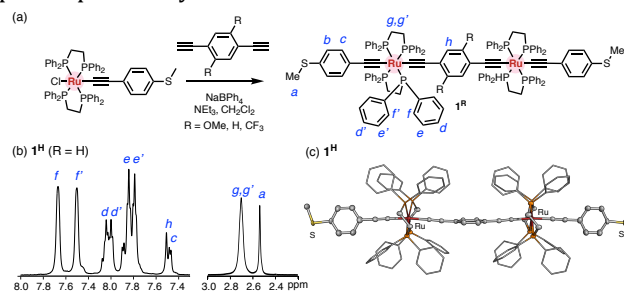

Figure 2. (a) Synthesis of **1^R** (R = OMe, H, CF$_3$). (b) A ^{1}H NMR spectrum of **1^H** observed at 500MHz in CDCl$_3$ at r.t. (c) The X-ray structure of **1^H** with a thermal ellipsoid plot of 50% probability. Phenyl rings in the dppe ligands are drawn with a wire model.

Preparation and Characterization of Monocationic Species [1^R][BARF].

To investigate the electrochemical properties of **1^R** (R = OMe, H, CF$_3$), cyclic voltammetry was performed. All the three complexes **1^R** exhibited two reversible well-separated oxidation waves in the range from 0 to –500 mV (vs. FeCp$_2$/FeCp$_2$$^+$ redox couple, Figure 3a). On the basis of the separation of the two redox waves (ΔE), the comproportionation constants (K_C) were determined to be 7.8 x 10^3 (**1^{CF3}**), 1.4 x 10^5 (**1^H**), and 1.8 x 10^6 (**1^{OMe}**). The large K_C values and the reversible redox waves indicate formation of the monocationic species [**1^R**]$^+$ thermodynamically stable in solutions.

Monocationic species [**1^R**][BARF] (R = H and OMe; BARF$^-$ = B$^-$(3,5-(CF$_3$)$_2$C$_6$H$_3$)$_4$) were synthesized by treatment of **1^R** dissolved in CH$_2$Cl$_2$ with 1 eq. of [FeCp$_2$][BARF], and were
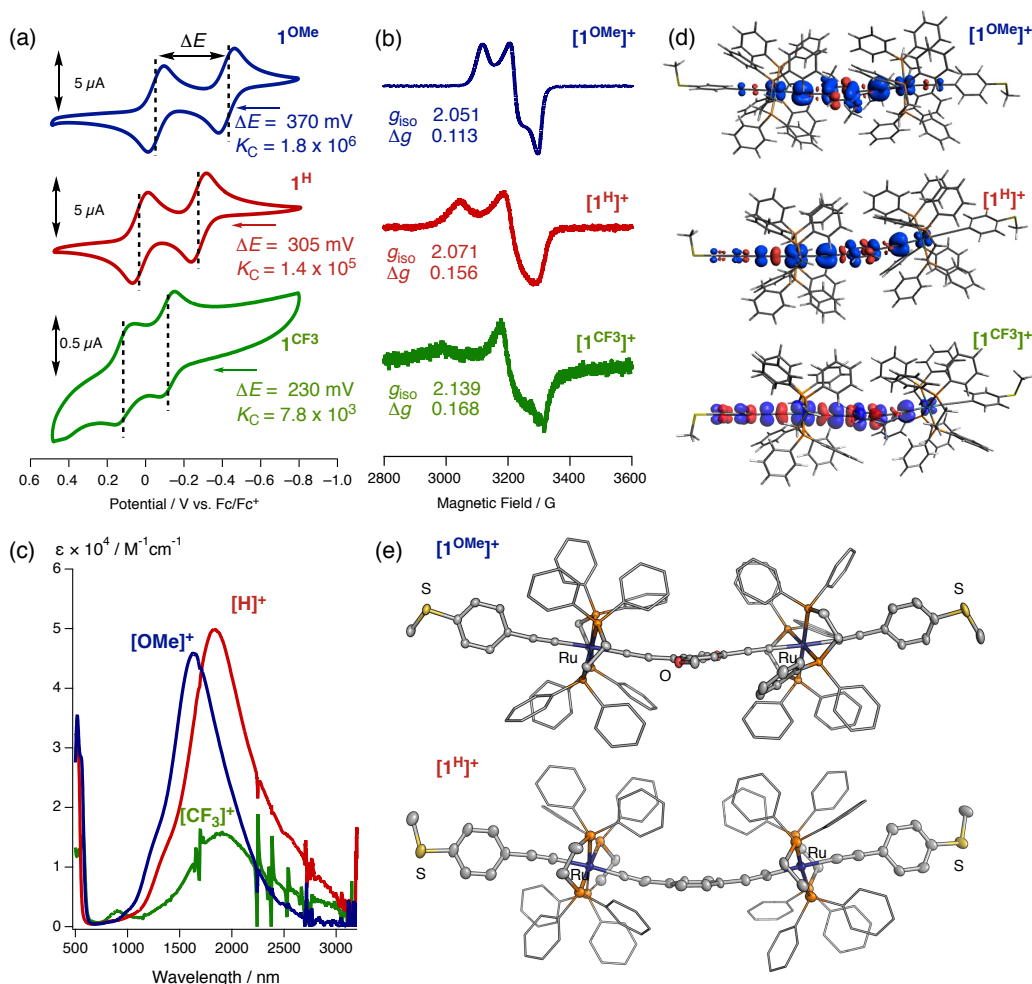
Figure 3. Physicochemical data for 1^R. (a) Cyclic voltammograms: 1^H and 1^{OMe}: 1.0 mM in CH_2Cl_2; 1^{CF3}: 0.1 mM in CH_2Cl_2 (0.1 mM [*n*-Bu$_4$N][PF$_6$], W.E and C.E : Pt, R.E : Ag/Ag$^+$, r.t.). (b) ESR spectra (113 K in CH_2Cl_2 glasses). (c) Vis-NIR spectra of [1^R]$^+$ (0.1 mM in CH_2Cl_2). (d) Spin density plots obtained by the DFT calculations (BLYP35-D3/Def2SVP,PCM(CH_2Cl_2)). (e) X-ray structures of the cationic parts of [1^{OMe}]$^+$ and [1^H]$^+$. Hydrogen atoms and solvents' molecules were omitted. Phenyl rings in the dppe ligands are depicted as the wire models.

isolated in 64 ([1^H][BARF]) and 95% isolated yields ([1^{OMe}][BARF]). Although our attempts to isolate [1^{CF3}][BARF] have not been successful yet probably due to its smaller K_C value, the monocationic species [1^{CF3}]$^+$ turned out to be stable in solution under ambient conditions (*vide supra*) and thus in the following measurements, [1^{CF3}]$^+$ was generated *in situ* by the treatment of 1^{CF3} with 1 eq. of [FeCp$_2$][BARF].

The monocationic species [1^R][BARF] were readily characterized by electron spin resonance (ESR) and near infrared (NIR) absorption spectroscopy (Figure 3b). ESR spectra of [1^R][BARF] observed at 113 K as CH_2Cl_2 glasses revealed rhombic signals typical of the Ru(dppe)$_2$ complexes with an unpaired spin. The isotropic parameters (g_{iso} = (g_1 + g_2 + g_3)/3; [1^{OMe}]$^+$ 2.051; [1^H]$^+$ 2.071; [1^{CF3}]$^+$ 2.139) are close to that for the free organic radical (g_{free} = 2.0023), and the split parameters (Δg) decrease with the electron-donating substituents ([1^{OMe}]$^+$ 2.051; [1^H]$^+$ 2.071; [1^{CF3}]$^+$ 2.139), suggesting that the 1e-oxidized cationic radical [1^{OMe}]$^+$ bears more contribution of the organic parts. In-

tense NIR absorptions observed for [1^R][BARF] (λ_{max} = 1656 ([1^{OMe}]$^+$), 1825 ([1^H]$^+$), 1903 nm ([1^{CF3}]$^+$)) should stem from the intramolecular Ru-Ru interaction in [1^R]$^+$ (Figure 3c). The absorptions disappear upon addition of excess amounts of [FeCp$_2$][BARF] due to formation of the corresponding dicationic species [1^R]$^{2+}$ (Figure S10).

The spin density distributions estimated by the DFT study reveal even distribution on the two Ru atoms for [1^{OMe}]$^+$ (0.15 : 0.15) and uneven distribution for [1^H]$^+$ (0.47 : 0.05) and [1^{CF3}]$^+$ (0.42 : 0.06, Figure 3d). Thus, complexes [1^H]$^+$ and [1^{CF3}]$^+$ are classified into charge-localized class II compounds, while the OMe derivative [1^{OMe}]$^+$ is a charge-delocalized class III compound.

Solid-state structures of [1^H][BARF] and [1^{OMe}][BARF] were characterized by X-ray diffraction study (Figure 3e). The diethynylbenzene moieties slightly distorted from the planarity ($\angle C_{Ar}$-C≡C = 168.5º). Compared to the neutral compound 1^H, the bonding features change from the acetylene structure Ru-C≡C-C$_{Ar}$ to the cumulenic structure Ru=C=C=C$_{Ar}$ as indicated by the shortening of the Ru-C

(2.033 Å) and $\equiv$C-C$_{Ar}$ bonds (1.425 Å) as well as the lengthening of the C$\equiv$C bonds ($d_{C\equiv Cav}$ = 1.217 Å) (cf. 1^H: d_{Ru-Cav} (2.050 Å), $d_{\equiv C-C Arav}$ (1.446 Å), $d_{C\equiv Cav}$ (1.223 Å)). In accord with the Robin-Day classification discussed above, the unsymmetrical bonding feature of the Ru-C$\equiv$C-Ar-C$\equiv$C-Ru moiety in $[1^H]^+$ is in contrast to the virtually symmetrical feature in $[1^{OMe}]^+$ (Tables S2, 3). This is also supported by the DFT study.
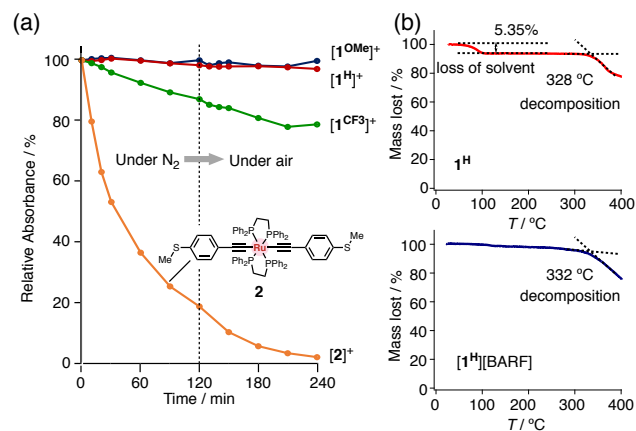

Figure 4. (a) Time-course plots of the Vis-NIR absorptions of $[1^R][BARF]$ (R = OMe, H, CF$_3$) in CH$_2$Cl$_2$ ([complex] = 0.1 mM). The experiments were performed under nitrogen atmosphere (from 0 to 120 min) and then the solutions were exposed to air. (b) TG thermograms of 1^H and $[1^H][BARF]$. The amount of the lost CH$_2$Cl$_2$ solvent for 1^H was in good agreement with the E.A data.

Stability and Reversibility of Switching Behavior.

High thermal stability of $[1^R]^+$ under ambient conditions is highlighted by the time-course analysis of the Vis-NIR absorptions of $[1^R][BARF]$ dissolved in CH$_2$Cl$_2$. The dinuclear complexes $[1^R][BARF]$ turned out to be stable for 2 h both under nitrogen atmosphere and in air as can be seen from the retention of the Vis-NIR absorptions (1^{OMe} 100%; 1^H 98%; 1^{CF3} 79%), whereas the mononuclear analogue **2** rapidly and almost completely decomposed under the same conditions (Figure 4a). These results proved that the dinuclear skeleton is one of effective methods to stabilize monocationic radical species containing the Ru(dppe)$_2$ fragment. Because the sequential treatment of 1^H with $[FeCp_2][BARF]$ and $FeCp*_2$ to 1^H caused reversible Vis-NIR spectral changes (Figure S11), the redox process can be repeated at least 6 times in solution.

Furthermore, thermogravimetric analysis of the neutral 1^H and cationic $[1^H][BARF]$ complexes revealed that they were stable up to around 300 ºC (Figure 4b). This high thermal stability in the solid-state should benefit device fabrication and switching operation in the nanogap.

STM-BJ Study. Using the STM-break junction (BJ) technique,[27] we measured single-molecule conductance of 1^R and $[1^R][BARF]$ in mesitylene (Figure 5a-c). The 1D histograms of both of the neutral and monocationic species reveal the conductance features in the range of 10^{-2}-10^{-6} G_0. The statistical analyses give the single-molecule conductance of the neutral and monocationic species as summarized in Table 1, and the conductance plot against the Hammett parameter σ[28] is shown in Figure 5d. The fea-

tures of the 2D histograms extended over 2.5 nm are consistent with the connection of $[1^R]^{n+}$ at the terminal thiomethyl anchor groups ($d_{S\cdots S}$ ~3.0 nm) when the snapback distance (~0.5 nm) are taken into account (Figures 5e,f, and S17a). The conductance of the neutral species increases by introduction of the electron-donating substituents (225-fold from 1^{CF3} to 1^{OMe}). Compared with molecular junctions composed of simple organic molecules such as phenylenediamine[29] and carbazole derivatives,[30] the large conductance change of 1^R induced by the substituents is remarkable. On the other hand, conductance of the monocationic species follows the opposite trend, i.e. conductance decrease from $[1^{CF3}]^+$ to $[1^{OMe}]^+$ by 0.4-fold. As a result, the ON/OFF switching ratio, which is relative ratio of the conductance of the monocationic species in relation to the neutral ones, drastically changes from 191 (for the CF$_3$ derivatives) to 48 (for the H derivatives) and then to 0.4 (for the OMe derivatives). This result shows that the organometallic molecular switch 1^R-$[1^R]^+$ can be facilely and effectively modulated by the substituents on the central aromatic rings.

We also carried out *in situ* switching experiments (Figure 5g). Addition of an equimolar amount of $[FeCp_2][BARF]$ to a mesitylene solution of 1^H caused a shift of the conductance peak to 10^{-3} G_0 suggestive of generation of $[1^H]^+$. Inversely, *in-situ* reduction of a mesitylene solution of $[1^H][BARF]$ by $FeCp*_2$ (Cp*; 1,2,3,4,5-pentamethylcyclopentadienyl) led to replacement of the conductance peak of $[1^H][BARF]$ with that around 10^{-5} G_0, which was superimposable on that of .1^H. Thus, the switching behavior could be reproduced reversibly in solution.

DFT-NEGF study. To gain insight into the tunable ON/OFF ratios, we carried out DFT-NEGF calculations on molecular junction models of $[1^{R'}]^{n+}$ (n = 0, 1) with truncated bis(dimethylphosphino)methane ligands with the Au clusters attached to the terminal thiomethyl groups (Figure 5h, i).[31–33] The HOMO transmission peaks of the neutral species are located close to the Fermi energy level (E_F) and are sensitive to the substituents. The HOMO transmission peaks approach to E_F, as the substituents become more electron-donating (CF$_3$ (–0.23 eV) → H (–0.10 eV) → OMe (–0.03 eV); highlighted as the square marks in Figure 4h) as is also supported by the HOMO energies estimated from the cyclic voltammograms (CF$_3$ (-4.93 eV) → H (-4.76 eV) → OMe (-4.61 eV)). Theoretically estimated conductance of $1^{OMe'}$ significantly increases compared to those of $1^{H'}$ and $1^{CF3'}$ because the HOMO transmission peak of $1^{OMe'}$ is closer to the Fermi level. Because slope of the transmission spectrum at E_F is steep, a small shift of the transmission peak energy leads to a large conductance change. By contrast, the HOMO-LUMO gaps of simple organic molecules are, in general, so large that the conduction peaks are located far apart from the Fermi level. As a result, the conductance around E_F becomes small to make the transmission curve around E_F flat and lead to the less sensitivity of the conduction to the substituents.
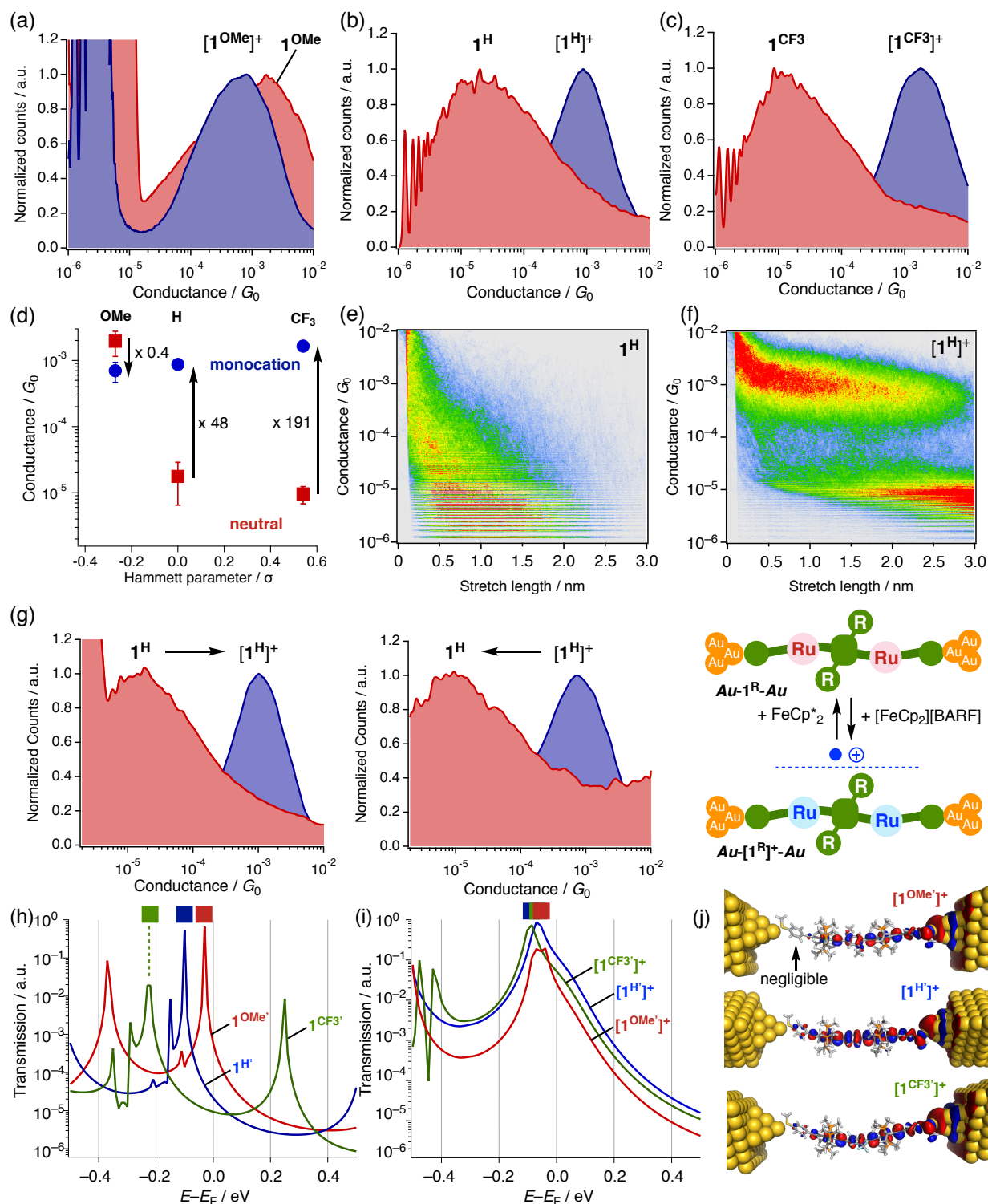
Figure 5. 1D histograms obtained by the STM-BJ study of (a) [1^{OMe}]$^{n+}$, (b) [1^H]$^{n+}$ and (c) [1^{CF3}]$^{n+}$ (n = 0,1). (d) Plots of conductance versus Hammett parameter. (e,f) 2D histograms of 1^H and [1^H][BARF]. (g) *In situ* oxidation of 1^H with [FeCp$_2$][BARF] and reduction of [1^H][BARF] with FeCp*$_2$. Transmission spectra for (h) the ***Au*-$1^{R'}$-*Au*** and (i) ***Au*-[$1^{R'}$]$^+$-*Au*** junctions (***Au***; Au cluster). Square marks indicate the dominant transmission peaks. (j) Dominant transmission eigenchannels at the Fermi level for the Au-[$1^{R'}$]$^+$-Au junctions.

Table 1. Experimental and theoretical conductance of $\mathbf{1^R}$ and $[\mathbf{1^R}]^+$.

R in $\mathbf{1^R}$ and $[\mathbf{1^R}]^+$	Experiment		ON/OFF ratio	DFT-NEGF	
	conductance / $\times 10^{-5} G_0$			conductance / $\times 10^{-5} G_0$	
	neutral ($\mathbf{1^R}$)	monocation ($[\mathbf{1^R}][BARF]$)		neutral ($\mathbf{1^{R'}}$)	monocation ($[\mathbf{1^{R'}}]^+$)
OMe	200 ($\pm$ 80)	71 ($\pm$ 44)	0.35	57	2050
H	1.8 ($\pm$ 1.1)	87 ($\pm$ 11)	48	2.2	10700
CF$_3$	0.89 ($\pm$ 0.28)	170 ($\pm$ 20)	191	0.96	4500

On the other hand, the energy levels of the transmission peaks of the monocationic species $[\mathbf{1^{R'}}]^+$ are in the very narrow range irrespective of R (Figure 5i). This phenomenon can be interpreted in terms of the *pinning effect*, i.e. the singly occupied orbital of open-shell species is placed at the energy level close to the Fermi energy. As a result, molecular junctions reveal conductance almost identical regardless of the molecular backbone.[34] However, the BJ study of the monocationic species revealed slight decrease of conductance by introduction of the OMe substituents (0.4-fold from $[\mathbf{1^{CF3}}]^+$ to $[\mathbf{1^{OMe}}]^+$). The trend is also suggested by the calculations; the conductance peak of $[\mathbf{1^{OMe'}}]^+$ is weaker than those of $[\mathbf{1^{H'}}]^+$ and $[\mathbf{1^{CF3'}}]^+$. According to the transmission eigenchannels (Figure 5j), the contribution of one of the two terminal anchor groups of $[\mathbf{1^{OMe'}}]^+$ (indicated with the arrow) is smaller than those of $[\mathbf{1^{H'}}]^+$ and $[\mathbf{1^{CF3'}}]^+$, suggesting that the weak electronic coupling between the molecule and the electrode.

Considering the Marcus-Hush regime, *the fact that the MV complexes shows similar conductance regardless of the charge-delocalized states* is against our expectation.[35–37] Highly charge-delocalized class III systems are expected to show high carrier mobility, while class II systems should show lower carrier mobility in solution and bulk solid state as well. However, our results suggest that, *in the single-molecule conductance, there is no apparent relationship between charge-delocalization and conductance, and even the trend is inversed i.e. the class II systems ($[\mathbf{1^H}]^+$ and $[\mathbf{1^{CF3}}]^+$) exhibit conductance higher than the Class III system ($[\mathbf{1^{OMe}}]^+$).* This discrepancy can be interpreted as follows: in the coherent tunneling process, interaction between the metal electrodes and the molecule dominates the conductance (pinning effect) rather than the intramolecular interaction. By contrast, the Marcus-Hush-type charge transfer phenomena deal with thermal activation processes accompanying solvent reorganization. Thus, significant MV character in molecular junction may appear when the conductance mechanism is dominated by thermally activated hopping process.[38]

Switching behavior in Nano-gap.

The switching function of the $\mathbf{1^R}/[\mathbf{1^R}]^+$ system was further studied by the nanogap technique. The conductance obtained by the STM-BJ technique is not for a specific molecule because after the break junction step another molecule comes into the electrodes and the process is repeated many times. So we can just obtain averaged features of molecules in the sample solution. In contrast to the *dynamic* STM-BJ technique, the *static* nanogap technique described below does not involve such BJ steps and molecules sandwiched between the nanogap stay there during the measurement so that we can observe changes of a particular molecules fixed between the electrodes. Therefore, we have chances to observe the switching process of fixed molecules induced by *in-situ* redox processes.

The 1 nm-sized nanogap **NG0** was prepared following the procedure reported previously.[39] The *I-V* characteristic of **NG**s obtained after immersion in $\mathbf{1^H}$ (**NG1$^\mathbf{H}$**) or $[\mathbf{1^H}][PF_6]$ solution (**NG[1$^\mathbf{H}$]$^+$**) revealed resistance of 7.96 GΩ (**NG1$^\mathbf{H}$**) and 1.61 GΩ (**NG[1$^\mathbf{H}$]$^+$**) at 0.1V, which were significantly smaller than the value obtained with a bare nanogap **NG0** (546 GΩ).[40] Furthermore, we performed surface enhanced Raman scattering (SERS) experiments of **NG1$^\mathbf{H}$** to confirm molecular finger print in the nanogap.[41–44] The Raman spectrum obtained from **NG1$^\mathbf{H}$** showed characteristic signals at 520, 1000, 1070, and 1175 cm^{-1}, which correspond to those observed for the bulk sample of $\mathbf{1^H}$ as compared in Figure 6b. The Raman mapping images provided high Raman intensity points at the nanogap (Figure 6b inset), supporting the molecular junction formation.

In situ ON/OFF experiment was performed for the nanogap containing $\mathbf{1^R}$ described above (**NG1$^\mathbf{H}$**). Immersion of **NG1$^\mathbf{H}$** in a CH$_2$Cl$_2$ solution of $[FeCp_2][BARF]$ gave **NG[1$^\mathbf{H}$]$^+$**, which showed the conductance increased by a factor of 42 (at 1V). This change should correspond to the formation of the nanogap containing $[\mathbf{1^H}]^+$-bridges. Recovery of the conductance was achieved by further treatment of **NG[1$^\mathbf{H}$]$^+$** with a mesitylene solution of FeCp*$_2$. Thus, this study demonstrated the ON/OFF switching behavior of the dinuclear molecular switch and its potential application for molecular devices.
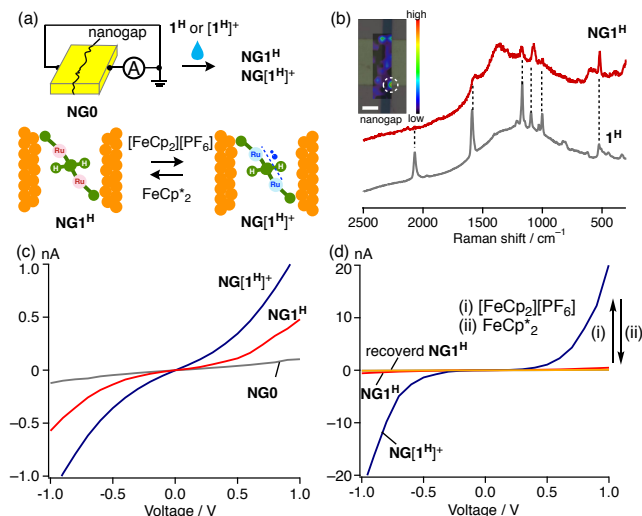
Figure 6. (a) Schematic images of preparation of nanogap junctions **NG1^H** and **NG[1^H]^+**, and *in situ* oxidation and reduction of **NG1^H** and **NG[1^H]^+**. (b) SERS spectra of **NG1^H** and bulk samples of **1^H**. The inset shows a Raman mapping image of **NG1^H**. The high Raman intensity point (highlighted by a circle) was observed in the nanogap. [45] The white scale bar indicates 10 μm. (c) *I-V* curves of **NG0, NG1^H and NG[1^H]^+**. (d) In situ ON/OFF switching experiments of **NG1^H** with sequential addition of [FeCp$_2$][PF$_6$] and FeCp*$_2$.

CONCLUSION

In summary, we have developed new organometallic molecular switches **1^R-[1^R]^+** responding to redox stimuli. Both of the neutral and monocationic MV complexes are stable under ambient conditions (at r.t. in air). It is notable that the monocationic species, otherwise usually unstable (in particular, mononuclear systems), are stabilized by the $d\pi$-systems delocalized widely over the Ru-C≡C-Ar-C≡C-Ru linkages to lead to the stable MV states. Single-molecule conductance study reveals that the molecules show switching behavior. Interestingly, the ON/OFF switching ratio can be facilely controlled by the substituents embedded into the bridging linkers up to a factor of *ca.* 200, mainly due to a drastic conductance change of the neutral species. This change is responsible for the high-lying HOMO orbitals caused by the electron-rich ruthenium fragments. We have also demonstrated the switching behavior in the nanogap, which shows potential application to device fabrication. Notably, this study presents a rare example of a single-molecule conductance study of the MV complexes,[46,47] and achievement of tunable ON/OFF ratio. Thus, we have revealed that the dinuclear organometallic system offers a new platform for a modulable molecular switch, which will open new molecular electronic fields.

AUTHOR INFORMATION

Corresponding Authors

Yuya Tanaka –
orcid.org/0000-0002-0674-660X; Email:
ytanaka@res.titech.ac.jp
Munetaka Akita –
orcid.org/ 0000-0001-7007-9621; Email: akitatit@icloud.com

REFERENCES

(1)   Kiguchi, M.; Ohto, T.; Fujii, S.; Sugiyasu, K.; Nakajima, S.; Takeuchi, M.; Nakamura, H. Single Molecular Resistive Switch Obtained via Sliding Multiple Anchoring Points and Varying Effective Wire Length. *J. Am. Chem. Soc.* **2014**, *136* (20), 7327–7332. https://doi.org/10.1021/ja413104g.

(2)   Pei, L.-Q.; Horsley, J. R.; Seng, J.-W.; Liu, X.; Yeoh, Y. Q.; Yu, M.-X.; Wu, X.-H.; Abell, A. D.; Zheng, J.-F.; Zhou, X.-S.; Yu, J.; Jin, S. Mechanically Induced Switching between Two Discrete Conductance States: A Potential Single-Molecule Variable Resistor. *ACS Appl. Mater. Interfaces* **2021**, *13* (48), 57646–57653. https://doi.org/10.1021/acsami.1c12151.

(3)   Li, J.; Shen, P.; Zhen, S.; Tang, C.; Ye, Y.; Zhou, D.; Hong, W.; Zhao, Z.; Tang, B. Z. Mechanical Single-Molecule Potentiometers with Large Switching Factors from Ortho-Pentaphenylene Foldamers. *Nat Commun* **2021**, *12* (1), 167. https://doi.org/10.1038/s41467-020-20311-z.

(4)   Li, Z.; Smeu, M.; Afsari, S.; Xing, Y.; Ratner, M. A.; Borguet, E. Single-Molecule Sensing of Environmental PH—an STM Break Junction and NEGF-DFT Approach. *Angew. Chem. Int. Ed.* **2014**, *53* (4), 1098–1102. https://doi.org/10.1002/anie.201308398.

(5)   Yoshihara, Y.; Fujii, S.; Higashibayashi, S.; Kiguchi, M.; Nishino, T. Single-Molecule Electric Switching Induced by Acid-Base Reaction. *Chem. Lett.* **2021**, *50* (6), 1271–1273. https://doi.org/10.1246/cl.210088.

(6)   Dulić, D.; van der Molen, S. J.; Kudernac, T.; Jonkman, H. T.; de Jong, J. J. D.; Bowden, T. N.; van Esch, J.; Feringa, B. L.; van Wees, B. J. One-Way Optoelectronic Switching of Photochromic Molecules on Gold. *Phys. Rev. Lett.* **2003**, *91* (20), 207402. https://doi.org/10.1103/PhysRevLett.91.207402.

(7)   Whalley, A. C.; Steigerwald, M. L.; Guo, X.; Nuckolls, C. Reversible Switching in Molecular Electronic Devices. *J. Am. Chem. Soc.* **2007**, *129* (42), 12590–12591. https://doi.org/10.1021/ja073127y.

(8)   Jia, C.; Migliore, A.; Xin, N.; Huang, S.; Wang, J.; Yang, Q.; Wang, S.; Chen, H.; Wang, D.; Feng, B.; Liu, Z.; Zhang, G.; Qu, D.-H.; Tian, H.; Ratner, M. A.; Xu, H. Q.; Nitzan, A.; Guo, X. Covalently Bonded Single-Molecule Junctions with Stable and Reversible Photoswitched Conductivity. *Science* **2016**, *352* (6292), 1443–1445. https://doi.org/10.1126/science.aaf6298.

(9)   Li, Y.; Baghernejad, M.; Qusiy, A.-G.; Zsolt Manrique, D.; Zhang, G.; Hamill, J.; Fu, Y.; Broekmann, P.; Hong, W.; Wandlowski, T.; Zhang, D.; Lambert, C. Three-State Single-Molecule Naphthalenediimide Switch: Integration of a Pendant Redox Unit for Conductance Tuning. *Angew. Chem. Int. Ed.* **2015**, *54* (46), 13586–13589. https://doi.org/10.1002/anie.201506458.

(10)   Yin, X.; Zang, Y.; Zhu, L.; Low, J. Z.; Liu, Z.-F.; Cui, J.; Neaton, J. B.; Venkataraman, L.; Campos, L. M. A Reversible Single-Molecule Switch Based on Activated Antiaromaticity. *Sci. Adv. 3* (10), eaao2615. https://doi.org/10.1126/sciadv.aao2615.

(11)   Chen, Y.; Huang, L.; Chen, H.; Chen, Z.; Zhang, H.; Xiao, Z.; Hong, W. Towards Responsive Single-Molecule Device. *Chin. J. Chem.* **2021**, *39* (2), 421–439. https://doi.org/10.1002/cjoc.202000420.

(12)   Li, Z.; Li, H.; Chen, S.; Froehlich, T.; Yi, C.; Schönenberger, C.; Calame, M.; Decurtins, S.; Liu, S.-X.; Borguet, E. Regulating a Benzodifuran Single Molecule Redox Switch via Electrochemical Gating and Optimization of Molecule/Electrode Coupling. *J. Am. Chem. Soc.* **2014**, *136* (25), 8867–8870. https://doi.org/10.1021/ja5034606.

(13)   Creutz, C.; Taube, H. Direct Approach to Measuring the Franck-Condon Barrier to Electron Transfer between Metal Ions. *J. Am. Chem. Soc.* **1969**, *91* (14), 3988–3989. https://doi.org/10.1021/ja01042a072.

(14)   Ren, T. Diruthenium σ-Alkynyl Compounds: A New Class of Conjugated Organometallics. *Organometallics* **2005**, *24* (21), 4854–4870. https://doi.org/10.1021/om050452q.

(15)   Lissel, F.; Schwarz, F.; Blacque, O.; Riel, H.; Lörtscher, E.; Venkatesan, K.; Berke, H. Organometallic Single-Molecule Electronics: Tuning Electron Transport through X(Diphosphine)2FeC4Fe(Diphosphine)2X Building Blocks by Varying the Fe–X–Au Anchoring Scheme from Coordinative to Covalent. *J. Am. Chem. Soc.* **2014**, *136* (41), 14560–14569. https://doi.org/10.1021/ja507672g.

(16)   Tanaka, Y.; Kiguchi, M.; Akita, M. Inorganic and Organometallic Molecular Wires for Single-Molecule Devices. *Chem. Eur. J.* **2017**, *23* (20), 4741–4749. https://doi.org/10.1002/chem.201604812.

(17)   Milan, D. C.; Vezzoli, A.; Planje, I. J.; Low, P. J. Metal Bis(Acetylide) Complex Molecular Wires: Concepts and Design Strategies. *Dalton Trans.* **2018**, *47* (40), 14125–14138. https://doi.org/10.1039/C8DT02103A.

(18)   Schwarz, F.; Kastlunger, G.; Lissel, F.; Egler-Lucas, C.; Semenov, S. N.; Venkatesan, K.; Berke, H.; Stadler, R.; Lörtscher, E. Field-Induced Conductance Switching by Charge-State Alternation in Organometallic Single-Molecule Junctions. *Nature Nanotech* **2016**, *11* (2), 170–176. https://doi.org/10.1038/nnano.2015.255.

(19)   For a molecular wire with a combination of redox and photoirradiation, see ref. 20.

(20)   Meng, F.; Hervault, Y.-M.; Shao, Q.; Hu, B.; Norel, L.; Rigaut, S.; Chen, X. Orthogonally Modulated Molecular Transport Junctions for Resettable Electronic Logic Gates. *Nat Commun* **2014**, *5* (1), 3023. https://doi.org/10.1038/ncomms4023.

(21)   Schauer, P. A.; Low, P. J. Ligand Redox Non-Innocence in Transition-Metal σ-Alkynyl and Related Complexes. *Eur. J. Inorg. Chem.* **2012**, *2012* (3), 390–411. https://doi.org/10.1002/ejic.201100995.

(22)   Tanaka, Y.; Akita, M. Organometallic Radicals of Iron and Ruthenium: Similarities and Dissimilarities of Radical Reactivity and Charge Delocalization. *Coord. Chem. Rev.* **2019**, *388*, 334–342. https://doi.org/10.1016/j.ccr.2019.02.036.

(23)   Fox, M. A.; Le Guennic, B.; Roberts, R. L.; Brue, D. A.; Yufit, D. S.; Howard, J. A. K.; Manca, G.; Halet, J.-F.; Hartl, F.; Low, P. J. Simultaneous Bridge-Localized and Mixed-Valence Character in Diruthenium Radical Cations Featuring Diethynylaromatic Bridging Ligands. *J. Am. Chem. Soc.* **2011**, *133* (45), 18433–18446. https://doi.org/10.1021/ja207827m.

(24)   Rigaut, S.; Perruchon, J.; Le Pichon, L.; Touchard, D.; Dixneuf, P. H. Synthesis of Ruthenium Acetylides: New Building Blocks for Molecular Electronics. *J. Organomet. Chem.* **2003**, *670* (1), 37–44. https://doi.org/10.1016/S0022-328X(02)02101-0.

(25)   Sugimoto, K.; Idei, H.; Tanaka, Y.; Akita, M. Synthesis and Charge Delocalization Property of Multimetallic Molecular Wires with Diethynylthiophene Bridges. *J. Organomet, Chem.* **2017**, *847*, 121–131. https://doi.org/10.1016/j.jorganchem.2017.02.033.

(26)   Tanaka, Y.; Kato, Y.; Sugimoto, K.; Kawano, R.; Tada, T.; Fujii, S.; Kiguchi, M.; Akita, M. Single-Molecule Junctions of Multinuclear Organometallic Wires: Long-Range Carrier Transport Brought about by Metal–Metal Interaction. *Chem. Sci.* **2021**, *12* (12), 4338–4344. https://doi.org/10.1039/D0SC06613C.

(27)   Xu, B.; Tao, N. J. Measurement of Single-Molecule Resistance by Repeated Formation of Molecular Junctions. *Science* **2003**, *301* (5637), 1221–1223. https://doi.org/10.1126/science.1087481.

(28)   Hansch, Corwin.; Leo, A.; Taft, R. W. A Survey of Hammett Substituent Constants and Resonance and Field Parameters. *Chem. Rev.* **1991**, *91* (2), 165–195. https://doi.org/10.1021/cr00002a004.

(29)   Venkataraman, L.; Park, Y. S.; Whalley, A. C.; Nuckolls, C.; Hybertsen, M. S.; Steigerwald, M. L. Electronics and Chemistry: Varying Single-Molecule Junction Conductance Using Chemical Substituents. *Nano Lett.* **2007**, *7* (2), 502–506. https://doi.org/10.1021/nl062923j.

(30)   Yzambart, G.; Rincón-García, L.; Al-Jobory, A. A.; Ismael, A. K.; Rubio-Bollinger, G.; Lambert, C. J.; Agraït, N.; Bryce, M. R. Thermoelectric Properties of 2,7-Dipyridylfluorene Derivatives in Single-Molecule Junctions. *J. Phys. Chem. C* **2018**, *122* (48), 27198–27204. https://doi.org/10.1021/acs.jpcc.8b08488.

(31)   Brandbyge, M.; Mozos, J.-L.; Ordejón, P.; Taylor, J.; Stokbro, K. Density-Functional Method for Nonequilibrium Electron Transport. *Phys. Rev. B* **2002**, *65* (16), 165401. https://doi.org/10.1103/PhysRevB.65.165401.

(32)   Tada, T.; Kondo, M.; Yoshizawa, K. Green's Function Formalism Coupled with Gaussian Broadening of Discrete States for Quantum Transport: Application to Atomic and Molecular Wires. *J. Chem. Phys.* **2004**, *121* (16), 8050–8057. https://doi.org/10.1063/1.1799991.

(33)   For detailed structures of molecular junction model, see SI.

(34)   Wang, K.; Vezzoli, A.; Grace, I. M.; McLaughlin, M.; Nichols, R. J.; Xu, B.; Lambert, C. J.; Higgins, S. J. Charge Transfer Complexation Boosts Molecular Conductance through Fermi Level Pinning. *Chem. Sci.* **2019**, *10* (8), 2396–2403. https://doi.org/10.1039/C8SC04199G.

(35)   Thomas, G. A.; Schafer, D. E.; Wudl, F.; Horn, P. M.; Rimai, D.; Cook, J. W.; Glocker, D. A.; Skove, M. J.; Chu, C. W.; Groff, R. P.; Gillson, J. L.; Wheland, R. C.; Melby, L. R.; Salamon, M. B.; Craven, R. A.; De Pasquali, G.; Bloch, A. N.; Cowan, D. O.; Walatka, V. V.; Pyle, R. E.; Gemmer, R.; Poehler, T. O.; Johnson, G. R.; Miles, M. G.; Wilson, J. D.; Ferraris, J. P.; Finnegan, T. F.; Warmack, R. J.; Raaen, V. F.; Jerome, D. Electrical Conductivity of Tetrathiafulvalenium-Tetracyanoquinodimethanide (TTF-TCNQ). *Phys. Rev. B* **1976**, *13* (11), 5105–5110. https://doi.org/10.1103/PhysRevB.13.5105.

(36)   Demadis, K. D.; Hartshorn, C. M.; Meyer, T. J. The Localized-to-Delocalized Transition in Mixed-Valence Chemistry. *Chem. Rev.* **2001**, *101* (9), 2655–2686. https://doi.org/10.1021/cr990413m.

(37)   Xie, L. S.; Sun, L.; Wan, R.; Park, S. S.; DeGayner, J. A.; Hendon, C. H.; Dincă, M. Tunable Mixed-Valence Doping toward Record Electrical Conductivity in a Three-Dimensional Metal–Organic Framework. *J. Am. Chem. Soc.* **2018**, *140* (24), 7411–7414. https://doi.org/10.1021/jacs.8b03604.

(38)   Ie, Y.; Okamoto, Y.; Inoue, T.; Seo, T.; Ohto, T.; Yamada, R.; Tada, H.; Aso, Y. Improving Intramolecular Hopping Charge Transport via Periodical Segmentation of π-Conjugation in a Molecule. *J. Am. Chem. Soc.* **2021**, *143* (2), 599–603. https://doi.org/10.1021/jacs.0c10560.

(39)   Naitoh, Y.; Ohata, T.; Matsushita, R.; Okawa, E.; Horikawa, M.; Oyama, M.; Mukaida, M.; Wang, D. F.; Kiguchi, M.; Tsukagoshi, K.; Ishida, T. Self-Aligned Formation of Sub 1 Nm Gaps Utilizing Electromigration during Metal Deposition. *ACS Appl. Mater. Interfaces* **2013**, *5* (24), 12869–12875. https://doi.org/10.1021/am403115m.

(40)   Probably Due to the Large Size of BARF Salt, No Resistance Change Was Observed before and after Immersion in [1H][BARF].

(41)   Nie, S.; Emory, S. R. Probing Single Molecules and Single Nanoparticles by Surface-Enhanced Raman Scattering. *Science* **1997**. https://doi.org/10.1126/science.275.5303.1102.

(42)   Suzuki, S.; Kaneko, S.; Fujii, S.; Marqués-González, S.; Nishino, T.; Kiguchi, M. Effect of the Molecule–Metal Interface on the Surface-Enhanced Raman Scattering of 1,4-Benzenedithiol. *J. Phys. Chem. C* **2016**, *120* (2), 1038–1042. https://doi.org/10.1021/acs.jpcc.5b10385.

(43)   Langer, J.; Jimenez de Aberasturi, D.; Aizpurua, J.; Alvarez-Puebla, R. A.; Auguié, B.; Baumberg, J. J.; Bazan, G. C.; Bell, S. E. J.; Boisen, A.; Brolo, A. G.; Choo, J.; Cialla-May, D.; Deckert, V.; Fabris, L.; Faulds, K.; García de Abajo, F. J.; Goodacre, R.; Graham, D.; Haes, A. J.; Haynes, C. L.; Huck, C.; Itoh, T.; Käll, M.; Kneipp, J.; Kotov, N. A.; Kuang, H.; Le Ru, E. C.; Lee, H. K.; Li, J.-F.; Ling, X. Y.; Maier, S. A.; Mayerhöfer, T.; Moskovits, M.; Murakoshi, K.; Nam, J.-M.; Nie, S.; Ozaki, Y.; Pastoriza-Santos, I.; Perez-Juste, J.; Popp, J.; Pucci, A.; Reich, S.; Ren, B.; Schatz, G. C.; Shegai, T.; Schlücker, S.; Tay, L.-L.; Thomas, K. G.; Tian, Z.-Q.; Van Duyne, R. P.; Vo-Dinh, T.; Wang, Y.; Willets, K. A.; Xu, C.; Xu, H.; Xu, Y.; Yamamoto, Y. S.; Zhao, B.; Liz-Marzán, L. M. Present and Future of Surface-Enhanced Raman Scattering. *ACS Nano* **2020**, *14* (1), 28–117. https://doi.org/10.1021/acsnano.9b04224.

(44)   We measured SERS measurement by the commercial laser Raman spectrometer (NRS 4500, JASCO Corporation, Japan). The wavelength and power of the excitation laser were 785 nm and 3 mW

(45)   The normal Raman spectrum of the **1^H** was obtained with the laser irradiation of 20 s. The intensity of the vibrational mode observed at 1175 cm^{-1} were mapped with the resolution of 3 μm. The mapping area is 12 μm x 42 μm.

(46)   Liu, I. P.-C.; Bénard, M.; Hasanov, H.; Chen, I.-W. P.; Tseng, W.-H.; Fu, M.-D.; Rohmer, M.-M.; Chen, C.; Lee, G.-H.; Peng, S.-M. A New Generation of Metal String Complexes: Structure, Magnetism, Spectroscopy, Theoretical Analysis, and Single Molecular Conductance of an Unusual Mixed-Valence Linear [Ni5]8+ Complex. *Chem. Eur. J.* **2007**, *13* (31), 8667–8677. https://doi.org/10.1002/chem.200700750.

(47)   Ting, T.-C.; Hsu, L.-Y.; Huang, M.-J.; Horng, E.-C.; Lu, H.-C.; Hsu, C.-H.; Jiang, C.-H.; Jin, B.-Y.; Peng, S.-M.; Chen, C. Energy-Level Alignment for Single-Molecule Conductance of Extended Metal-Atom Chains. *Angew. Chem. Int. Ed.* **2015**, *127* (52), 15960–15964. https://doi.org/10.1002/ange.201508199.